EARTH SURFACE PROCESSES AND LANDFORMS, VOL 22, 1001–1025 (1997)

PROPERTIES OF A CELLULAR BRAIDED-STREAM MODEL

A. BRAD MURRAY[1]* AND CHRIS PAOLA[2]

[1]*Institute for Geophysics and Planetary Physics, University of California, San Diego, 9500 Gillmon Drive, La Jolla, CA 92093, USA*
[2]*Department of Geology and Geophysics, School of Earth Sciences, University of Minnesota*

Received 27 June 1995; Revised 16 January 1997; Accepted 27 January 1997

ABSTRACT

We have shown in a previous paper that many of the main features of braided streams can be captured in a relatively simple cellular computer model. Here we examine some of the detailed characteristics of this model. We show the qualitative form of the braiding produced by the model is generally insensitive to changes in most of the numerical parameters used in the model. The most crucial parameter choice is the use of a non-linear exponent (>1) to describe the relation between sediment flux and local stream power. Use of water discharge instead of stream power to parameterize sediment flux produces braiding, but also unrealistically high-amplitude topography variations in the long term. Introduction of a threshold transport condition causes no noticeable change in the model's behaviour. Inclusion of lateral sediment transport due to gravitational effects on lateral slopes is not crucial to produce braiding, but is needed to provide reasonable lateral channel shifting, and to maintain a continuing dynamic behaviour. As long as lateral sediment transport is included, altering the initial topography for a run has no effect, other than a transient period of regrading. In addition, we show that there is a simple and apparently fundamental connection between braided-stream channel networks and erosional (dendritic) networks that has not been previously recognized. All that is needed to switch the model from braided to dendritic patterns is either to remove redeposition from the rules, simulating entrainment of cohesive sediment, or to add a cliff to the initial topography, making local redeposition unimportant. This result suggests that the presence or absence of significant local redeposition, which causes bar formation, channel division, and avulsion, determines whether a braided or dendritic pattern will form.

Earth surf. process. landforms, **22,** 1001–1025 (1997)
No. of figures: 15 No. of tables: 1 No. of refs: 32
KEY WORDS: braided river; sediment transport; cellular; computer model; dendritic; erosion.

INTRODUCTION

Braided rivers are common in the world today and may have been the predominant river type during the Earth's early history. An active braided river exhibits a fascinating, complex dynamics in which water and sediment flow shift continuously from one part of the system to another. The river pattern, although perhaps stable in some averaged sense, is constantly reconfiguring itself. What are the essential physics of this dynamics? Recently we (Murray and Paola, 1994) proposed a simple cellular model for braiding that includes only bedload sediment transport driven by water flow that is routed over local topography (Figure 1). We intentionally left out many of the details of real rivers. Instead, we have retained only the most basic features in an effort to discover the processes essential to braided systems. One of the main purposes of developing such a model is to examine the sensitivity of the braided pattern to changes in the governing parameters and to inclusion of various physical processes that are known to occur in real river systems. In this paper, we report on systematic tests of the model under various conditions.

Our model is a variation of the cellular automata or coupled map lattice models of dynamical-systems research. Dynamical-systems/chaos theory shows that simple interactions can produce complex, apparently stochastic behaviour (Guckenheimer and Holmes, 1983). Recently, researchers (Tetzlaff and Harbaugh, 1989; Anderson, 1990; Chase, 1992; Forrest and Haff, 1992; Werner and Fink, 1993; Werner and Hallet, 1993) have applied this lesson to the formation of spatial patterns, using models that are relatives of the cellular automata developed in dynamical-systems research (Wolfram, 1984). Such models have been termed 'coupled map lattice' (CML) models by Kaneko (1993).

* Correspondence to: A. B. Murray

CCC 0197-9337/97/111001–25 $17.50

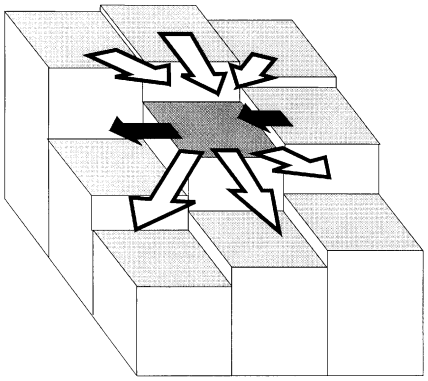

Figure 1. Schematic illustration of the rules in the cellular model. Open arrows show water and sediment routing (Q and Q_s rules in the text). Black arrows show lateral sediment transport (Q_l rule in the text).

Both CML models and typical numerical methods of solving partial differential equations share the characteristic that the solution is determined on a spatial grid based on some approximation to the governing equations. Solving a differential equation involves discretizing a set of equations believed to correctly represent the physics to a high level of approximation if they could be solved exactly. The locations of all surfaces at which boundary conditions are to be applied must be specified at each time step.

In a CML model, the physics are embedded in the model via a series of rules specifying how the cells in the lattic interact. CML models are especially useful for systems with spacially complex, self-organized patterns. In these cases, specification of boundary conditions needed to solve differential equations as the system evolves becomes extremely difficult. For example, in a braided river the shape of the boundaries is complex and changes continuously through time. A formulation that requires imposing some sort of spatial pattern as a condition of the analysis (e.g. the sinusoidal perturbations typically used in stability analyses) restricts the form of the patterns that can develop. Using a cellular model provides the freedom for the system to evolve spatially and form complex patterns without constraint. In addition, if the goal is to learn what minimal conditions are needed to produce a given pattern, then the possible difficulty of including all the details of the underlying physics in a CML model does not pose a significant problem.

METHOD

Our cellular model includes only a very simple representation of water flow and sediment transport. We have described the algorithm briefly elsewhere (Murray and Paola, 1994). Here we describe the method in greater detail.

Lattice and basic variable

The lattice is typically tens of cells wide by hundreds or thousands of cells long. For instance, in the runs shown in Figure 2 the lattice is 22 by 500. The real variables defined on the lattice are bed elevation, water discharge and sediment discharge. These and all other model parameters are specified in arbitrary units; we will discuss scaling relations among these units below. Most runs (exceptions discussed below) start with a uniform slope plus white-noise elevation perturbations with a range on the order of the elevation difference between adjacent rows of cells in the downhill direction (100 000 arbitrary units). We define a slope from one cell to another to be positive if the elevation of the first cell is greater than that of the second.

Water routing

Each iteration begins with the introduction of approximately 10 000 arbitrary units of water per cell in some or all of the cells at the upstream end of the lattice. The water moves downstream row by row. Although the units can represent volumes of water, they can as well be thought of as discharges, since they are a volume moved per

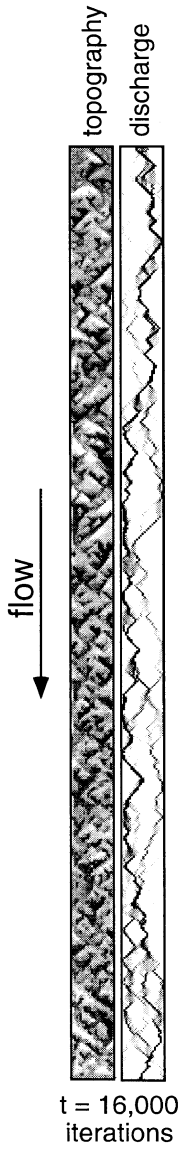

Figure 2. Output of the cellular model showing 22×500 cells. Darker shades indicate lower elevations and higher discharges. The overall slope has been removed before plotting the elevations. This run used $n = 0{\cdot}5$, Q_s rule 3 with $m = 2{\cdot}5$, $C_s = 300\,000$ (three times the average elevation difference between rows), and $K = 10^{-21}$. $K_l = 10^{-7}$ in the lateral sediment-transport (Q_l) rule.

iteration. We will use the terms 'amount of water' and 'discharge' interchangeably when discussing the model. We apply to each cell an algorithm that distributes the water in that cell to one or more of the three immediate neighbour cells in the next row downstream, with the most water going where the slope is greatest. If the slope(s) to any or all of these neighbours is (are) positive, we distribute water to that (those) cells according to the following rule (Figure 1):

$$Q_i = \frac{S_i^n}{1 / \sum_j \left(s_j\right)^n} Q_0 \qquad (Q \text{ rule 1a})$$

where Q_0 is the amount of water in the cell in question (cell 0), Q_i is the amount of water transferred from cell 0

to one of its immediate downstream neighbour cells (cell i), n is a constant which we discuss below, and S_i is the slope from cell 0 to cell i. Slopes equal the elevation differences between cells, divided by $2^{1/2}$ for diagonal neighbours. The sum, which runs over the downstream immediate-neighbour cells with positive slopes, normalizes the discharges so that all of the water entering a cell (cell 0) leaves it during that iteration.

Field and laboratory observations indicate that ponding does not occur often in braided rivers; either a positive surface slope or flow momentum usually drives the water up a negative bed slope. We do not include ponding in the model. If none of the slopes from cell 0 to the three immediate downstream neighbour cells is positive, we distribute water to all three of the neighbours, with more water going to the cells with the least uphill slopes, according to:

$$Q_i = \frac{S_i^{-n}}{1 / \sum_j S_j^{-n}} Q_0 \qquad (Q \text{ rule 1b})$$

where the sum is over all three downstream neighbours. If the slopes to all three of the immediate downstream neighbours are 0 (a rare occurrence), we distribute the water in cell 0 into all three evenly. In real braided streams, some of the discharge in a channel can flow uphill even though downhill options exist to the sides (e.g. on bar heads). This can occur in our model on scales larger than a cell width; if a channel is several cells wide, the slopes from cells at the bar head can all be negative, allowing uphill flow, even though water in adjacent cell flows downhill around the bar.

These water distribution rules represent a crude approximation to momentum conservation. The form of rule 1 can be derived from the equation of motion for uniform flow (a flow with no spatial accelerations) in a wide channel:

$$\tau = \rho g h S \qquad (1)$$

where τ is the shear stress the flow exerts on the bed, ρ is the density of water, g is the acceleration of gravity, h is water depth and S is the surface slope of the flow. Combining this with the relationship between τ and a representative flow velocity V (Vernard and Street, 1961):

$$\tau = f \rho V^2 / 8 \qquad (2)$$

(where f is a friction factor that depends on roughness and Reynolds number), we get:

$$V = C h^{1/2} S^{1/2}, \qquad (3)$$

where $C = 8g/f$ is the Chezy coefficient, which can be expressed as:

$$C = h^{1/6} / N \qquad (4)$$

where Manning's N depends on roughness, and we have used the approximation that for a wide flow h can be substituted for R_h, the hydraulic radius (Vernard and Street, 1961). Using Equations 3 and 4 and the expression:

$$Q = hV \qquad (5)$$

for the discharge per unit width Q, we have:

$$Q = h^{5/3} S^{1/2} / N \qquad (6)$$

We do not claim that Equation 6 is a good local approximation throughout a braided river network, but are simply using it to obtain a reasonable value (1/2) for the exponent n in Q rule 1. In the model, we distribute

parcels of water into downstream neighbour cells, so in the rule we replace the coefficient *1/N* with a term that normalizes the discharges to that all the water in a cell moves into the next row downstream during each iteration.

Sediment routing

The water transports sediment from cell to cell according to one of six different rules we have used, which involve the local discharge or the local stream power index, *QS*:

$$Q_{si} = K[Q_i]^m \qquad (Q_s \text{ rule 1})$$

$$Q_{si} = K[Q_i S_i]^m \qquad (Q_s \text{ rule 2})$$

$$Q_{si} = K[Q_i(S_i + C_s)]^m \qquad (Q_s \text{ rule 3})$$

$$Q_{si} = K\left[Q_i S_i + \varepsilon \sum_{j=1}^{3} Q_{uj} S_{uj}\right]^m \qquad (Q_s \text{ rule 4})$$

$$Q_{si} = K[Q_i(S_i + C_s) - Th]^m \qquad (Q_s \text{ rule 5})$$

$$Q_{si} = K\left[Q_i S_i + \varepsilon \sum_{j=1}^{3} Q_{uj} S_{uj} - Th\right]^m \qquad (Q_s \text{ rule 6})$$

(We presented Q_s rules 1–4 in Murray (1994).) Q_{si} is the amount of sediment transported from the cell in question into one of the three downstream immediate neighbours, and K and m are constants.

We use Q_s rule 1 only to test the effect of using discharge to determine sediment flux. Q_s rule 2, which is somewhat more realistic, relates sediment transport to the local stream power index. While the stream power is not the most common parameter used to predict sediment load, empirical studies have related these quantities (Bagnold, 1980; Ashmore, 1985). Ashmore (1985) plots sediment discharge versus stream power index for several laboratory and field braided streams. Our standard value for the exponent m in these rules is 2·5, which comes from approximating the slope of a log–log plot of these quantities for Ashmore's (1985) series of laboratory braided stream runs. In addition, sediment-transport formulas involving bed shear stress τ can be expressed in a form involving stream power. Multiplying both sides of Equation 1 by V and using Equation 2 we have:

$$\tau^{3/2} = k_1 QS \tag{7}$$

where $k_1 = f^{1/2}\rho^{3/2}g/8$. Assuming relative roughness (depth divided by grain size) is approximately constant and the Reynolds number is high enough that its effect on f is negligible, k_1 can be treated as a constant. If sediment concentration $Q_s/(Q_s+Q)$ is approximated as Q_s/Q, the Engelund and Hansen (1967) sediment-transport formula, which we choose for its simplicity, can be expressed as:

$$Q_s = k_2 \tau^{5/2} \tag{8}$$

where k_2 is a constant. Combining this with Equation 7 leads to:

$$Q_s = k_3 (QS)^{5/3} \tag{9}$$

where k_3 is a constant. The sediment-transport formula developed by Graf (1971) can also be expressed in this form. We have done runs using a value of 5/3 for m (see the Results section below).

We choose a value for the constant K in Q_s rule 2 that occupies the position of k_3 based on practical considerations. If K in any of the sediment-transport rules is too large, a numerical instability results because large amounts of sediment move in one iteration, leading to deep holes and high hills on the cell scale. The excessive slopes between these features cause increasingly large amounts of sediment to move during successive iterations. If K is small enough to avoid this instability, decreasing it further does not appear to affect the behaviour of the model: it only makes the patterns develop more slowly, since then less material moves in each iteration. To minimize run times, we choose a value of K that is as large as possible without producing the instability.

Q_s rules 3 and 4 are two attempts to get around a problem with determining local sediment transport using Q_s rule 2. Ashmore (1985) related sediment transport to stream power for whole-river data, involving the total sediment and water discharges, and the average slope of a reach. Braided streams commonly have flat or negative bed slopes locally, and Q_s rule 2 predicts no sediment transpot in these cases. (Sediment transport in a direction opposite to the flow is not allowed.) Transport can occur on negative bed slopes in real flows (Lysne, 1969), because either a positive water surface slope or momentum drives the flow across such areas. Locally, the surface slope should be used to determine stream power, but in the model we are limited to using bed slopes. In Q_s rules 3 and 4 we add a term that allows sediment transport when the bed slope is zero or negative. In Q_s rule 3, C_s is a constant (on the order of the average elevation difference between rows), so that the added term is proportional to the local discharge. This gives the physically reasonable result that on a given negative slope, a larger discharge will produce a larger sediment flux. In Q_s rule 4 the term involves a sum of the stream powers entering a cell. Q_{uj} and S_{uj} are the discharges and slopes into the cell in question from the three upstream immediate-neighbour cells, and ε is a constant. Our standard value for ε is 0·35. This added term can be thought of as crudely representing the inertia of the flow, which is larger when the discharges and/or slopes leading into a cell are larger. Neither the constant of proportionality in Q_s rule 3, C_s, or the parameter ε in Q_s rule 4 are well constrained. The values we use for these constants make the added terms the same order of magnitude as a typical local stream power.

Q_s rules 5 and 6 incorporate a sediment-transport threshold, as do most sediment-transport formulas. This threshold, $Th, = Q_t S_t / ThD$, where Q_t is a typical discharge (that introduced into cells in the first row), S_t is a typical slope (the average elevation difference between rows), and the threshold denominator, ThD, is a constant. $ThD = 2$ in most runs in which we use rules 5 or 6, so that the threshold is around half of the typical stream power.

In real flows, if the bed has a slope that is not parallel to the local flow direction, such as near the banks of a channel, gravity produces a transverse component to the bedload sediment transport (Parker, 1976; Blondeaux and Seminara, 1985). To incorporate this effect, we apply to each cell containing discharge an algorithm that transports a small amount of sediment from lateral-neighbour cells that have higher elevations. This occurs regardless of whether these neighbour cells contain discharge, so that any channel bank can erode. The black arrows in Figure 1 illustrate this rule, which is based on an expression given explicitly by Parker (1984) for the transverse component of sediment flux q_{sl}:

$$q_{sl} = \frac{1 + \mu r}{\mu} \left(\frac{\tau_c}{\tau} \right)^{1/2} S_l q_s \tag{10}$$

where l denotes the transverse direction, r is the ratio of lift coefficient to drag coefficient, μ is the dynamic coefficient of Coulomb friction, τ_c is the critical value of τ, and q_s is the total local sediment flux. We neglect the dependence on τ, producing our lateral sediment-transport rule:

$$Q_{sl} = K_l S_l Q_{s0} \qquad (Q_l \text{ rule})$$

where Q_{sl} is the amount of sediment transported from a lateral-neighbour cell into the cell in question, S_l is the lateral slope, Q_{s0} is the total sediment load out of the cell in question into the three downstream immediate

neighbours, and K_l is a constant adjusted so that Q_{sl} is on the order of a few per cent of Q_{s0} for typical values of S_l, consitent with Equation 10.

Elevation changes

The model algorithm applies the water-routing and sediment-transport rules to each cell in a row (row $_l$), giving the discharges and amount of sediment entering each of the cells in the next row downstream (row $_{l+1}$). Then the algorithm applies these rules to the cells in row $_{l+1}$, giving the amount of sediment leaving each cell in row $_{l+1}$. Then, if the lateral sediment-transport rule is included, it is applied to each cell in row $_{l+1}$. The amount of sediment that enters each cell because of this rule is summed with the amount of sediment entering that cell from row $_l$. And the amount that leaves that cell because of the lateral transport rule is summed with the amount that leaves if for row $_{l+2}$. We then adjust the elevations of each cell in row $_{l+1}$, according to the difference between the total amount of sediment entering and leaving:

$$\Delta Elev = Q_s^{in} - Q_s^{out}. \qquad \text{(Elev. rule 1)}$$

This rule discretizes the two-dimensional Exner equation:

$$\frac{\partial \eta}{\partial t} = \frac{1}{1-\lambda} \nabla_{\mathrm{H}} (\vec{q}_s) \qquad (11)$$

where η is bed elevation, λ is the porosity of the deposit, ∇_H is the horizontal gradient, and $\vec{q}_s$ is the sediment flux vector. In the model, we neglect the dependence on deposit porosity, treating it as a constant. As we discuss in the section on scaling below, the constant K in the sediment-transport rules is not tightly constrained, so K can in effect absorb a constant factor related to porosity. Thus the sediment-transport rules can be thought of as giving a volume transported per iteration that is equal to the volume of the sediment plus the pore volume of the subsequent deposit.

This process of water and sediment transport and elevation changes repeats row by row until the water reaches the downstream end of the lattice, when the iteration ends.

Boundary conditions

In a standard run, we include high side walls to contain the flow. The walls are two columns wide because the inner column can erode if the lateral-transport rule is included. Experiments using periodic boundary conditions in the transverse direction, in which discharge is allowed to leave one side and re-enter the other, give qualitatively the same results as those using side walls. In most runs we fix the elevations of the first and last rows of cells, simulating the rigid end walls of laboratory experiments. In effect, in each iteration the algorithm replaces the sediment removed from the first row.

Altering discharge and slope

Adjusting the discharge or slope in the model is not straightforward. For example, if we doubled the number of discharge units introduced in cells in the first row at the start of each iteration, it would change the amount of sediment transferred by each application of the sediment-transport rule by the same amount. This change would be equivalent to changing K. The same is true of changing the slopes by changing the number of elevation units between rows of cells. We can, however, change the discharge in a more physically meaningful way by changing the number of cells in the first row that receive discharge.

Typical parameter values

Table I. Values of main parameters

Q	10 000
S	100 000
Q_s	1000
n	0·5
m	2·5
K	10^{-21}
K_l	10^{-7}
C_s	300 000
ε	0·35
Th	10^9

SCALING

Interpreting the units in the model, such as those for water and sediment discharges, is not straightforward, because the model has no intrinsic length and time scales. In real rivers, the grain size provides an externally imposed length scale. In the cellular model, however, we do not explicitly include grain size. In addition, the amount of time represented by an iteration cannot be set without reference to a length scale. In this section, we will outline one approach to interpreting the units in the model.

First, we will show that a standard scaling approach falls short when applied to the cellular model. If we could determine what (if any) kind of real river the model simulates, we could pick a prototype river to compare the model with. Characteristic values for discharges and slopes scale as:

$$Q \propto L^2R/T,\ Q_s \propto L^2R/T,\ S = H/L$$

where L, H, R and T are characteristic length, height, depth (or channel relief) and time scales, respectively. For example, the average value of the total width (the sum of the widths of all channels at a cross-section) could be used for L, the average vertical distance between places L apart in the overall downstream direction for H, and the average topographic channel depth for R. In terms of ratios of prototype to model quantities:

$$S_r = H_r/L_r \tag{12}$$

$$Q_r = Q_{sr} = L_r^2R_r/T_r \tag{13}$$

where, for example, $Q_r = Q_p/Q$, and Q_p and Q are typical discharges in the prototype model. Then, using the relationship between the stream power index (QS) and sediment transport:

$$Q_s = K(QS)^m \tag{14}$$

leads to

$$Q_{sr} = K_r(Q_rS_r)^m \tag{15}$$

where K_r is the ratio between the sediment-transport constant in the prototype and that in the model. Since this constant depends on relative roughness and Reynolds number, this ratio is not necessarily unity.

Two of the variables in these equations, H_r and R_r, are not independent. H and R are different characteristic vertical scales in real streams; as H gets larger (larger slopes), R generally decreases (shallower channels) (Parker, 1978). The ratios H_r and R_r between a model and a prototype will not necessarily have the same values. However, either H_r or R_r could determine the vertical scale of a model. In the context of the cellular braided-stream model, either H_r or R_r will determine what the elevation units (e.u.) in the model represent, and therefore the ratios are proportional to each other. Thus there are six independent variables (L_r, H_r (or R_r), T_r, S_r, K_r and

$Q_r = Q_{sr}$) and three equations (12, 13 and 15). The model system is under-constrained. To compare the model with a prototype, we must assign values to three of these ratios, and then determine the others.

In other words, the best we can do is to choose a prototype real stream and arbitrarily assume that the model scales like the prototype in some ways – that the model depicts a stream with the same size, slope and sediment-transport constant K as the prototype, for instance. Having chosen $L_r = S_r = K_r = 1$, Equation 12 gives H_r (and therefore R_r), Equation 15 gives Q_r (or Q_{sr}), and Equation 13 determines T_r.

As a concrete example, we will make such a comparison between the run of the model shown in Figure 2 and run 8 of Ashmore's laboratory experiments (Ashmore, 1985). Ashmore reports: the average total width, L_p, $=1{\cdot}06$ m; the average bed topographic relief index (used here for R_p) $=0{\cdot}00772$ m; S_p, $=0{\cdot}010$ (giving H_p $=1{\cdot}06\times0{\cdot}010\,\text{m}=0{\cdot}0106\,\text{m}$); $Q_p = 0{\cdot}0045\,\text{m}^3\text{s}^{-1}$; and $Q_{sp} = 8{\cdot}54\,\text{g s}^{-1}$, or $3{\cdot}2\times10^{-6}\,\text{m}^3\text{s}^{-1}$ (using a sediment density of $2{\cdot}65\,\text{g cm}^{-3}$).

For the model run shown in Figure 2, $L = 5$ cell widths (the average number of cells per cross-section with a discharge greater than 3 per cent of the total discharge in this analysis). We measured the bed relief index as defined by Ashmore (1985), giving $R \approx 1\times10^5$ e.u. $H = 5\times10^5$ e.u. (L multiplied by the average elevation difference between rows). A total of $1{\cdot}5\times10^4$ discharge units was introduced in the first row of cells.

Choosing $L_r = 1$ means that five cell widths $= 1{\cdot}06$ m; one cell width $= 0{\cdot}2$ m. Then $S_r = 1$ and Equation 12 gives $H_r = 1$, or 5×10^5 e.u. $= 0{\cdot}0106$ m; 1 e.u. $= 2{\cdot}1\times10^{-8}$ m. R_r follows, since $R = 1\times10^5$ e.u. $\times$ ($2{\cdot}1\times10^{-8}$ m/1 e.u.) $= 0{\cdot}0021$ m; $R_r = 0{\cdot}00772\,\text{m}/0{\cdot}0021\,\text{m} = 3{\cdot}8$. Equations 13 and 15 give $Q_r = Q_{sr} = 1$, so that $1{\cdot}5\times10^4$ discharge units $= 0{\cdot}0045\,\text{m}^3\text{s}^{-1}$.

The sediment transport constants for the laboratory stream and the model are, using Equation 14 and $m = 2{\cdot}5$:

$$K_p = 3{\cdot}2\times10^{-6}/(0{\cdot}0045\times0{\cdot}01)^{2{\cdot}5}\, s^{1{\cdot}5}/m^{4{\cdot}5} = 2{\cdot}4\times10^{13}\, s^{1{\cdot}5}/m^{4{\cdot}5}$$

$$K = 10^{-21}(\text{e.u.})^{-4}(\text{cell width})^{-0{\cdot}5}(\text{iterations})^{1{\cdot}5}$$

in the units natural to each system. Using $K_r = 1$ and the conversions between metres and e.u. and cell widths leads to:

$$K_p = K;\ 2{\cdot}4\times10^{13}\, s^{1{\cdot}5}/m^{4{\cdot}5} = 10^{-21}\ (\text{e.u.})^{-4}(\text{cells})^{-0{\cdot}5}(\text{iterations})^{1{\cdot}5}$$

or

$$2{\cdot}4\times10^{13}\, s^{1{\cdot}5}/m^{4{\cdot}5} = 1{\cdot}2\times10^{10}\ \text{iterations}^{1{\cdot}5}/m^{4{\cdot}5},\ \text{or 1 iteration} = 160\ \text{s}.$$

This analysis, while not rigorous, points out that the choice of K implicitly determines how much time an iteration represents, when the model is compared with a particular real braided stream.

RESULTS

We have described the dynamical behaviour of the model and how the patterns develop from an even slope with random elevation perturbations for four sediment-transport relationships (Murray and Paola, 1994). Here we will present some new results and explore in greater depth the sensitivity of the model output to changes in the rules.

Varying the sediment-transport rules; main results

A: the effect of non-linear dependence on discharge. Most combinations of rules and parameters produce basic braiding – a dynamically changing spatial pattern with flow divisions and confluences. The most essential requirement for braiding in the model is $m > 1$, where m is the exponent in the sediment-transport rules. This causes the excess scour and deposition that drive braiding in the model. We can most easily describe this instability in the context of starting a run with an initial slope plus random elevation perturbations, using Q_s rule 1, in which sediment transport depends on discharge. Low areas will gather more of the flow than their

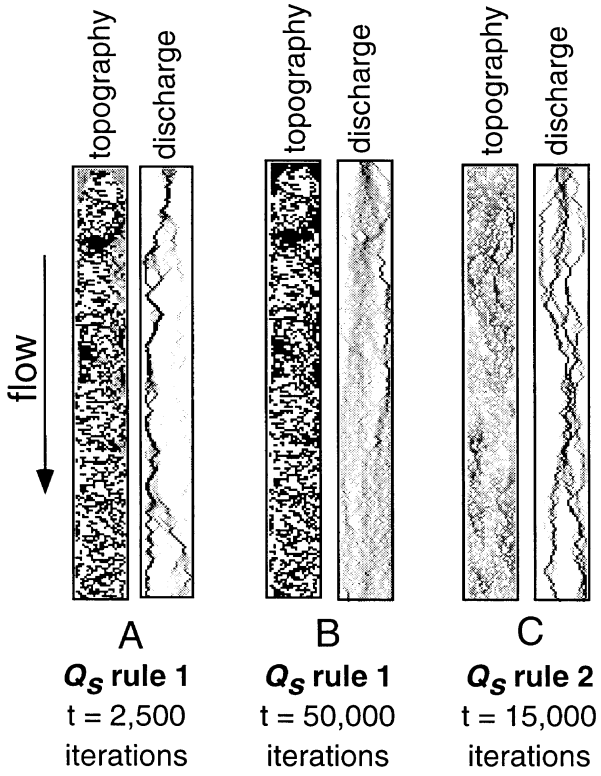

Figure 3. Model runs using Q_s rules 1 and 2, showing 22×250 cells. Darker shades indicate lower elevations and higher discharges. The overall slope has been removed before plotting the elevations. The juxtaposed very light and dark shades show much greater local relief than in runs using other sediment-transport rules. The Q_s rule 1 run used $n=0{\cdot}5$, $m=2{\cdot}5$, $K=10^{-7}$, and $K_l=10^{-7}$ in the lateral sediment-transport (Q_l) rule. The Q_s rule 2 run used $n=1{\cdot}5$, $m=2{\cdot}5$, $K=10^{-20}$, random initial topography perturbations with an amplitude of 600 000 elevation units (in most runs we use an amplitude of 200 000), and the Q_l rule is not included.

surroundings. If $m>1$ the sediment flux out of such a convergence will be greater than the sum of the fluxes into it from its surroundings. Thus a low area will get lower. A similar instability causes areas that are slightly higher than their surroundings to become higher, by causing flow divergences that lead to convergences in the sediment flux. The sediment removed from a deepening low area will be deposited downstream in an area where the flow diverges, and the deposition will likely cause stronger flow divergence, possibly leading to a split in the flow. In the model, the early-forming scour holes and deposits eventually concentrate the flow into the channels of a fully braided network (e.g. Figure 3A). We, as well as other workers (Hong and Davies, 1979; Ashmore, 1985), have observed laboratory-scale braided-streams developing in this way. These two instabilities continue to operate in a fully developed model run, driving the continual changes in spatial pattern.

Figure 4A shows the flow and topography after a few iterations of a run we conducted to illustrate these instabilities. A sinusoidally constricting channel forces the flow to converge and then diverge, and the channel bed is an even slope with no pertubations. Figure 4B shows the development after approximately 1000 iterations. As the channel narrows, the local nature of the water-routing rules causes flow convergence to occur most strongly along the walls before spreading into the middle of the channel farther downstream. Where the flow converges the sediment flux diverges and erosion results. Where the flow diverges just downstream of the constriction, deposition occurs. If this run were continued, the lateral transport rule would cause noticeable bank erosion and widening in some parts of the channel.

B: the effect of the dependence on slope. Q_s rule 1 illustrates how the non-linear relationship between discharge and sediment flux causes erosion and deposition. This rule, however, leads to out-of-control positive

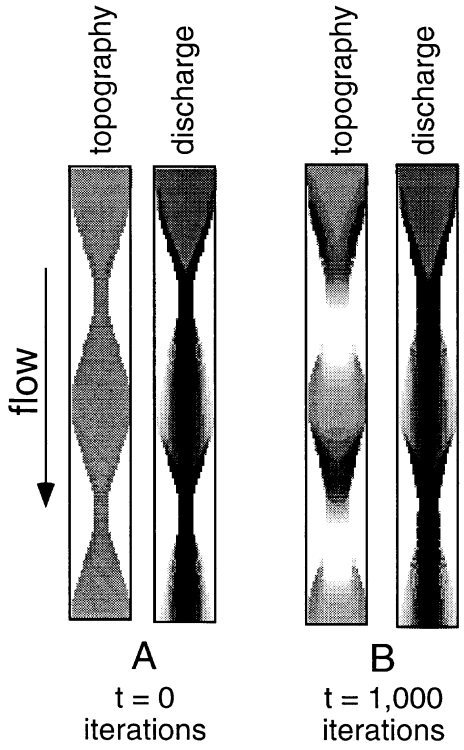

Figure 4. A model run starting with a smooth, sinusoidally narrowing channel, showing 34×200 cells. Darker shades show lower elevations and larger discharges. The overall slope has been removed before plotting the elevations. The image after 1000 iterations shows scour where the flow converges and deposition where it diverges. This run used $n = 0{\cdot}5$ and Q_s rule 3 with $m = 2{\cdot}5$, $C_s = 300\,000$, $K = 10^{-21}$, and $K_l = 10^{-7}$ in the lateral-sediment-transport (Q_l) rule. Runs with this initial topography using other Q_s rules develop in qualitatively the same way.

feedback as a run continues. Nothing in this rule increases sediment transport on steep slopes, or decreases it on negative slopes, so high places continue to get higher as low places get lower. Eventually, the topography becomes a very unrealistic collection of spires and deep holes (Figure 3B). In Q_s rule 2, inclusion of the slope dependence tends to increase the sediment transport into a hole while decreasing or eliminating the sediment transport out of the hole. Similarly, transport onto a hill is decreased or eliminated while transport off a hill is increased. Thus the slope dependence has a diffusive effect, encouraging holes to fill and hills to erode. This effect can be strong enough to overcome the instabilities described above that result from the discharge dependence, causing the initial perturbations to shrink rather than grow, leading to a progressively smoother bed rather than the channels of a braided network. Q_s rule 2 will lead to a braided network if three conditions are met: (1) the exponent n in Q rule 1 must be at least 1 (higher values of this exponent cause stronger flow convergence and divergence from a given topography); (2) the lateral sediment-transport rule must not be included (since that adds to the diffusive tendency); and (3) the range of the initial topography perturbations must be at least several times the average elevation difference between rows of cells (since larger elevation differences cause stronger flow convergence and divergence). (For most combinations of rules, the details of the initial topography make no difference to the development. With Q_s rule 2, however, we find that they do have a significant effect. This case is reminiscent of dynamical systems that exhibit chaotic behaviour only if the initial conditions differ significantly from those that lead to some simple behaviour.) Figure 3C shows the pattern that results from Q_s rule 2 under these conditions. As with Q_s rule 1, the topography resulting from Q_s rule 2 under these conditions is not realistic, featuring many bars that are small compared to the channel sizes. Q_s rules 1 and 2 are not meant as analogues of real behaviour, but they illustrate the effects of each of the physical processes added one at a time.

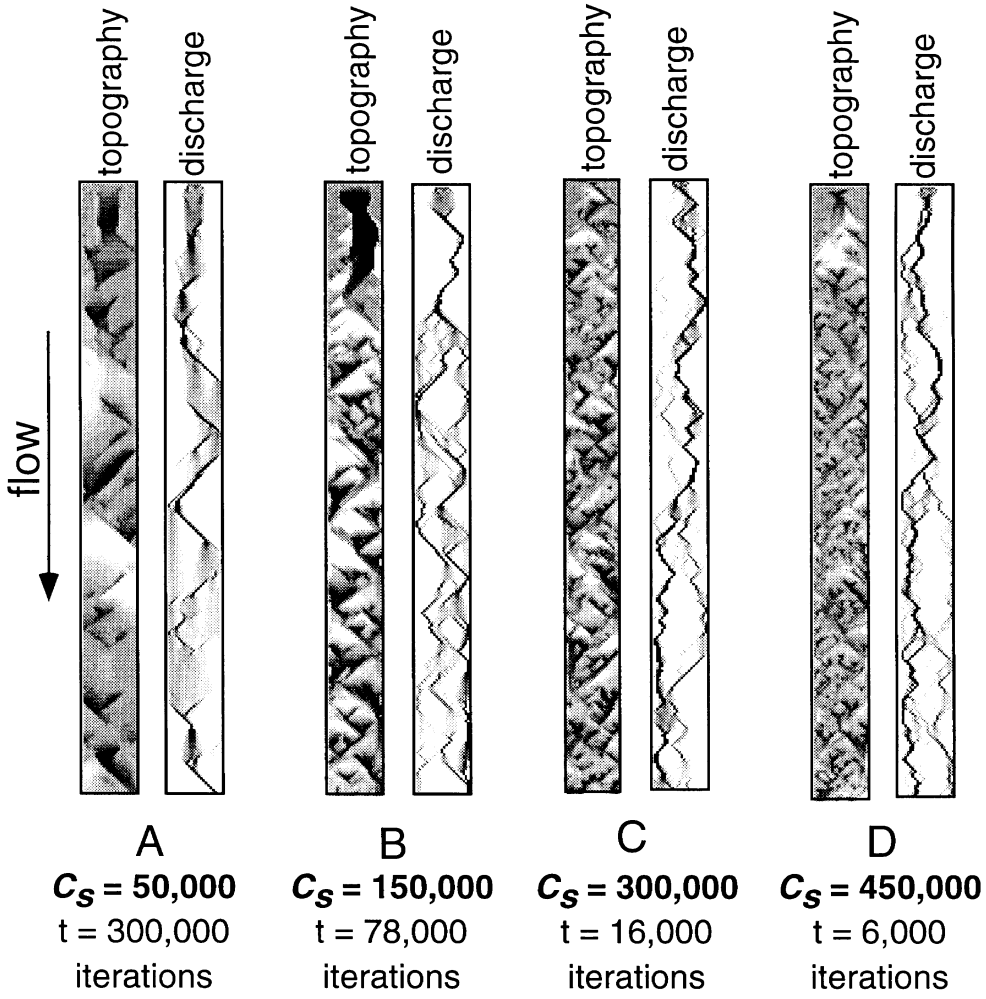

Figure 5. A series of model runs showing the effect of varying C_s in Q_s rule 3, showing 22×250 cells. Darker shades indicate lower elevations and higher discharges. The overall slope has been removed before plotting the elevations. These runs used $n=0{\cdot}5$, $m=2{\cdot}5$, $K=10^{-21}$, and $K_l=10^{-7}$ in the lateral-sediment transport (Q_l) rule. (Figure 2 is repeated here as (C)).

C: the effect of sediment transport on flat and uphill slopes. Q_s rules 3 and 4 are more physically realistic than Q_s rule 2, including a term representing flow momentum or positive surface slopes that allow uphill sediment transport. The results of runs using these rules generally appear more realistic as well, as Figures 5 and 6 show. These figures illustrate the results of changing the magnitude of the term added to the stream power in each of these rules. If this term is small enough, the patternsn are not realistic, as Figures 5A and 6A show. If C_s in Q_s rule 3 is larger, as in Figure 5C and 5D ($C_s=300\,000$ and 450 000 respectively), a qualitatively realistic braided network develops. These images show that increasing C_s in this range has little effect on the resulting pattern. Changing ε produces similar effects. Figure 6A shows the low-amplitude topography and fairly evenly spread discharge that results from a small value of ε (0·2), and Figure 6B–6D shows the qualitatively realistic patterns resulting from larger values of ε (0·35, 0·5 and 1). Again, the outcome of the model does not depend sensitively on this parameter within this range.

D: the effect of a sediment-transport threshold. Surprisingly, addition of the sediment-transport threshold in Q_s rule 5 does not affect the qualitative results, regardless of its magnitude, as long as it is not large enough to prevent transport altogether in the first iteration. Figure 7A shows the result of a run using this rule with a threshold that is half of a typical stream power (the threshold denominator, $ThD=2$). The pattern of Figure 7A

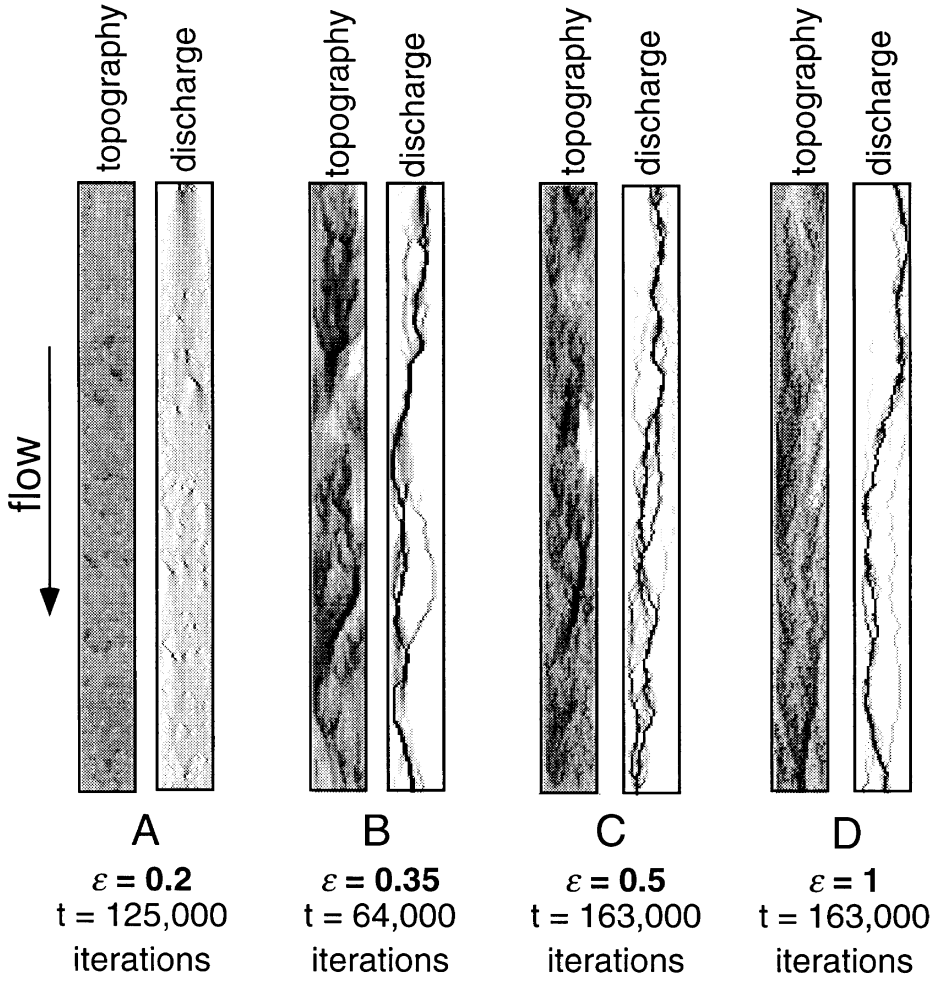

Figure 6. A series of model runs showing the effect of varying ε in Q_s rule 4, showing 22×250 cells. Darker shades indicate lower elevations and higher discharges. The overall slope has been removed before plotting the elevations. These runs used $n=0{\cdot}5$, $m=2{\cdot}5$, $K=10^{-21}$ (except the run shown in (A), which used $K=10^{-20}$), and $K_l=10^{-7}$ in the lateral-sediment-transport (Q_l) rule.

appears qualitatively the same as that shown in Figure 5C, which shows a run that differed only in the absence of a threshold (Q_s rule 3). The threshold in Q_s rule 6 produces an effect not observed in Q_s rule 5. If ε is fairly low and $ThD=2$, the intial perturbations are damped, as is shown in Figure 7B (ε=0·35). In the run shown in Figure 7C, ε is higher (ε=1), and channel development takes place. When a run starts with elevation perturbations on a flat surface, the flow is initially distributed over most of the bed, and stream powers are therefore low in most places. Because the term added to the stream power in Q_s rules 4 and 6 is a sum of the stream powers upstream of a cell, this term also will initially be small in most places. Where the local slope is negative, unless the slopes upstream are large, the weighted sum of local and upstream powers will be less than the threshold. The diffusive influence of the slope in the local stream power prevents any deep holes or high bars from developing. Using a larger value of ε increases the size of the term that does not depend on the local slope, making uphill sediment transport more likely, overcoming he diffusive tendency, and allowing development to proceed. As is the case for Q_s rule 5, the fully developed pattern is not very sensitive to the addition of a threshold, as a comparison of Figures 7C and 6 shows.

E: the effect of lateral transport. When the lateral transport (Q_l) rule is not included, channels are narrower (Figure 8A) and migrate less. We have recently run the model for millions of iterations. We have discovered

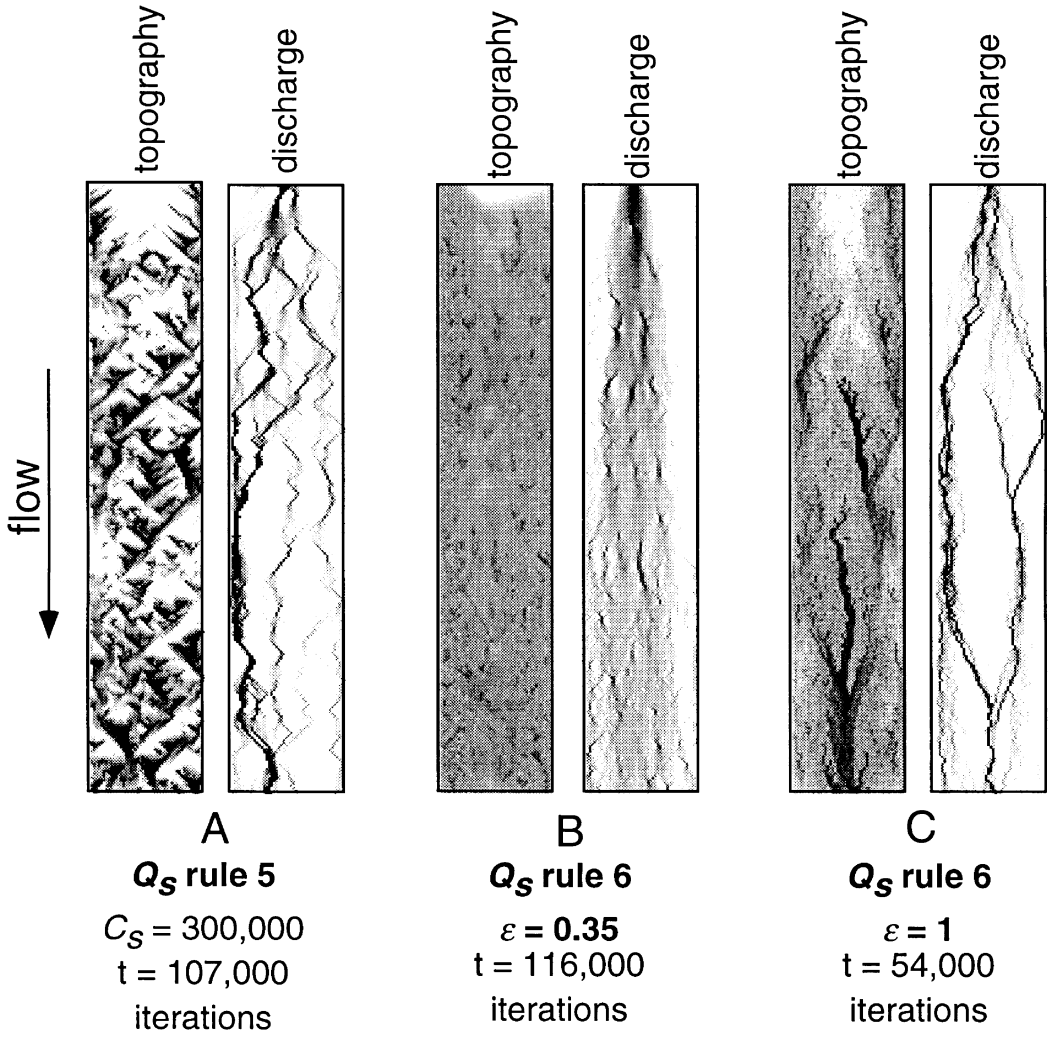

Figure 7. Model runs using Q_s rules 5 and 6, showing 50×250 cells. Darker shades indicate lower elevations and higher discharges. The overall slope has been removed before plotting the elevations. These runs used $n=0{\cdot}5$, $m=2{\cdot}5$, $K=10^{-21}$, $ThD=2$, and $K_l=10^{-7}$ in the lateral-sediment-transport (Q_l) rule.

that excluding the Q_l rule has a more fundamental effect in the very long term; the lateral sediment-transport rule is essential for the model to continue indefinitely to exhibit the complex dynamics involving channel switching and channel shifting. Without this rule, regardless of what other rules and parameters are used, the model eventually digs a deep canyon one to a few cells wide. Confining the flow in this way renders local redeposition ineffective at causing changes in the channel pattern. A very large amount of material would have to be redeposited to cause an avulsion in a deep canyon, and there is no room in a narrow canyon for bars to grow and divert the flow. Thus, without the Q_l rule, the model reaches a static steady state (Figure 8B).

We believe lateral sediment transport does play an important role in perpetuating the dynamic behaviour of braided streams, as this result suggests. However, this result is also partially an artifact of the inlet and outlet effects of the model. The fixed-elevation last row of lattice cells does not act as a fixed base level as it would for a real system. Because the water can climb hills and ponding is not included, base level can become arbitrarily low locally. The water can always climb a hill at the outlet. The area immediately below the inlet is prone to flow convergence that digs deep holes (as in Figure 5). If the Q_l rule is included, it delivers material from the walls of such an incised section, widening it until there is room in the bottom for braiding to occur. If the Q_l rule is not

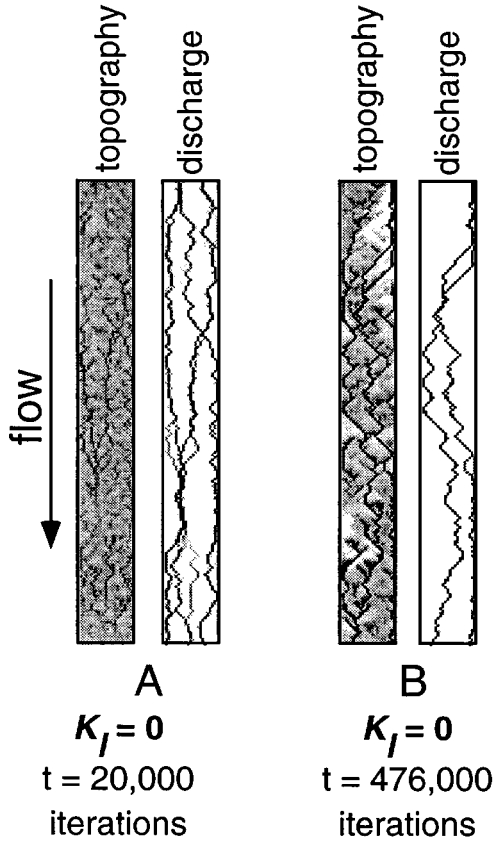

Figure 8. A model run without the lateral-sediment-transport (Q_l) rule, showing 22×200 cells. Darker shades indicate lower elevations and higher discharges. The overall slope has been removed before plotting the elevations. This run used $n=0{\cdot}5$, Q_s rule 3 with $m=2{\cdot}5$, $C_s=300\,000$, $K=10^{-21}$, and $K_l=10^{-7}$ in the lateral-sediment-transport (Q_l) rule. (A) After 20 000 iterations the model is still braiding. (B) After 400 000 iterations, channels have become incised for the length of the lattice.

included, incised sections never get any wider once they have captured the flow. Even without the Q_l rule, the model will exhibit metastable dynamic braiding for up to hundreds of thousands of iterations before an incised section lowers local base level and propagates a canyon for the length of the lattice.

Varying exponents

Figure 9 shows the effects of changing n in the Q rules (when Q_s rule 3 is used for sediment transport). If the Froude number of a real flow is high enough (>1), no influences can be transmitted upstream. In this case a value of 0 for n in the model may be appropriate; the flow would not respond to the elevations of the cells downstream in that case. The run shown in Figure 9A used $n=0$. The only distinction the Q rule makes in this case is between uphill and downhill. Figure 9A shows that the model still braids under these conditions, although the flow spreads into unrealistically unchannelled regions. The water has little tendency to gather in this case. Field and laboratory observations indicate that locally the flow does respond to different slopes in the different directions downstream, with more water going where the slope is greatest. Figure 9B–9D shows that as long as n is at least $0{\cdot}5$, this exponent has little effect on patterns the model produces when Q_s rule 3 is employed.

Figure 10 shows the effects of using Q_s rule 3 and changing m. In the run shown in Figure 10A, which used $m=0{\cdot}9$, the initial topography perturbations are damped, leading to progressively lower-amplitude undulations in the bed. This illustrates that this exponent must be greater than one to initiate the instabilities described at the beginning of this section, which lead to the development of braiding. The run shown in Figure 10B used $m=1{\cdot}67$, which is the value suggested by the use of uniform-flow approximations to express established

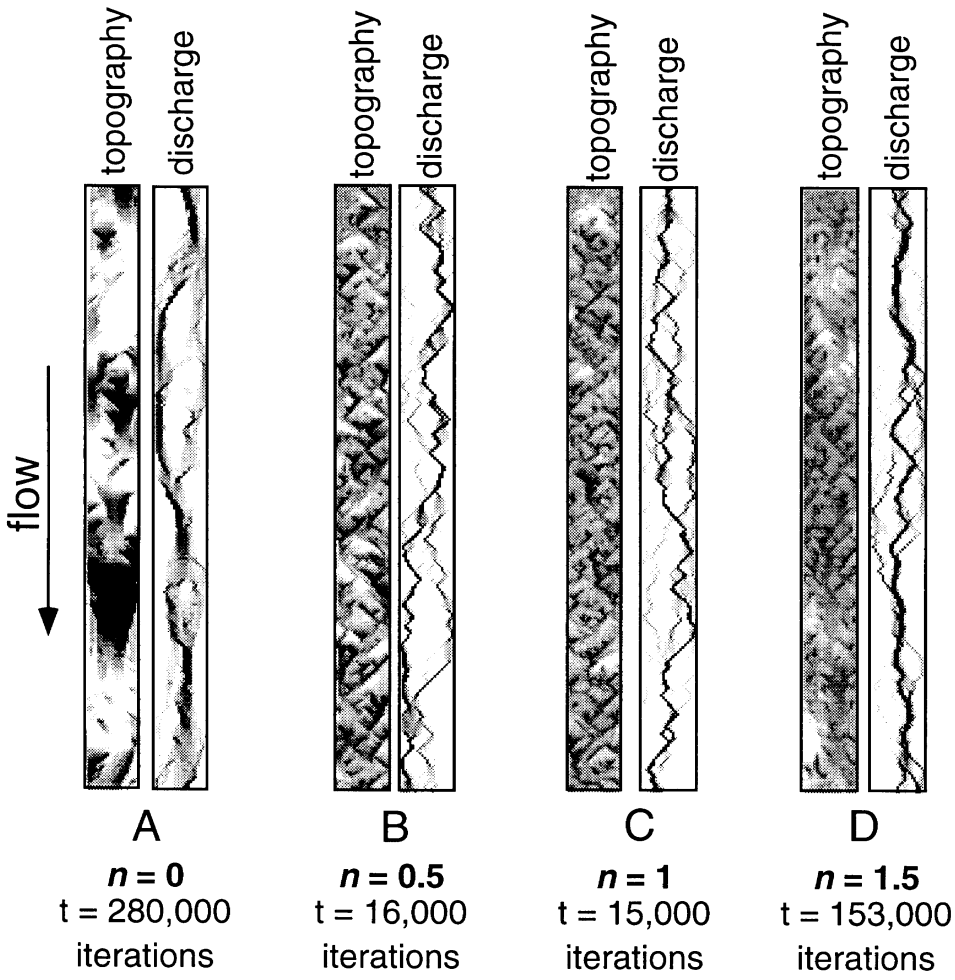

Figure 9. A series of model runs showing the effect of varying n in the water routing (Q) rule, showing 22×250 cells. Darker shades indicate lower elevations and higher discharges. The overall slope has been removed before plotting the elevations. These runs used Q_s rule 3 with $m=2{\cdot}5$, $C_s=300\,000$, $K=10^{-21}$, and $K_l=10^{-7}$ in the lateral-sediment-transport (Q_l) rule.

sediment-transport formulas in terms of stream power. This value leads to a pattern that is somewhat more regular and less realistic than the empirical value of 2·5, as a comparison of Figure 10B and 10C shows. Changing m to higher values does not significantly alter the results (Figure 10D and 10E).

Changing the width/depth ratio

As was briefly reported in Murray and Paola (1994), we have done a series of runs that test whether the model reproduced the results of linear stability analyses. Here we present the outcome of this experiment. Linear stability analyses predict that the number of initially forming, infinitesimal-amplitude bars in a cross-section increases linearly with the width/depth ratio of the flow (Parker, 1976; Fredsoe, 1978). For a given depth and a moderate relative roughness, a flow about 16 depths wide produces alternating bars and a meandering thalweg (Figure 11A), a flow twice as wide produces some bars in the middle of the channel and thus a thalweg that splits and rejoins (Figure 11B), and a flow twice as wide as this produces twice as many bars and thalwegs per cross-section (Figure 11C).

In the model experiment, we change the width of the confining channel while introducing water in all the cells in the first row in each case. Thus, in the initial flow the discharge in each cell (which we use as a proxy for

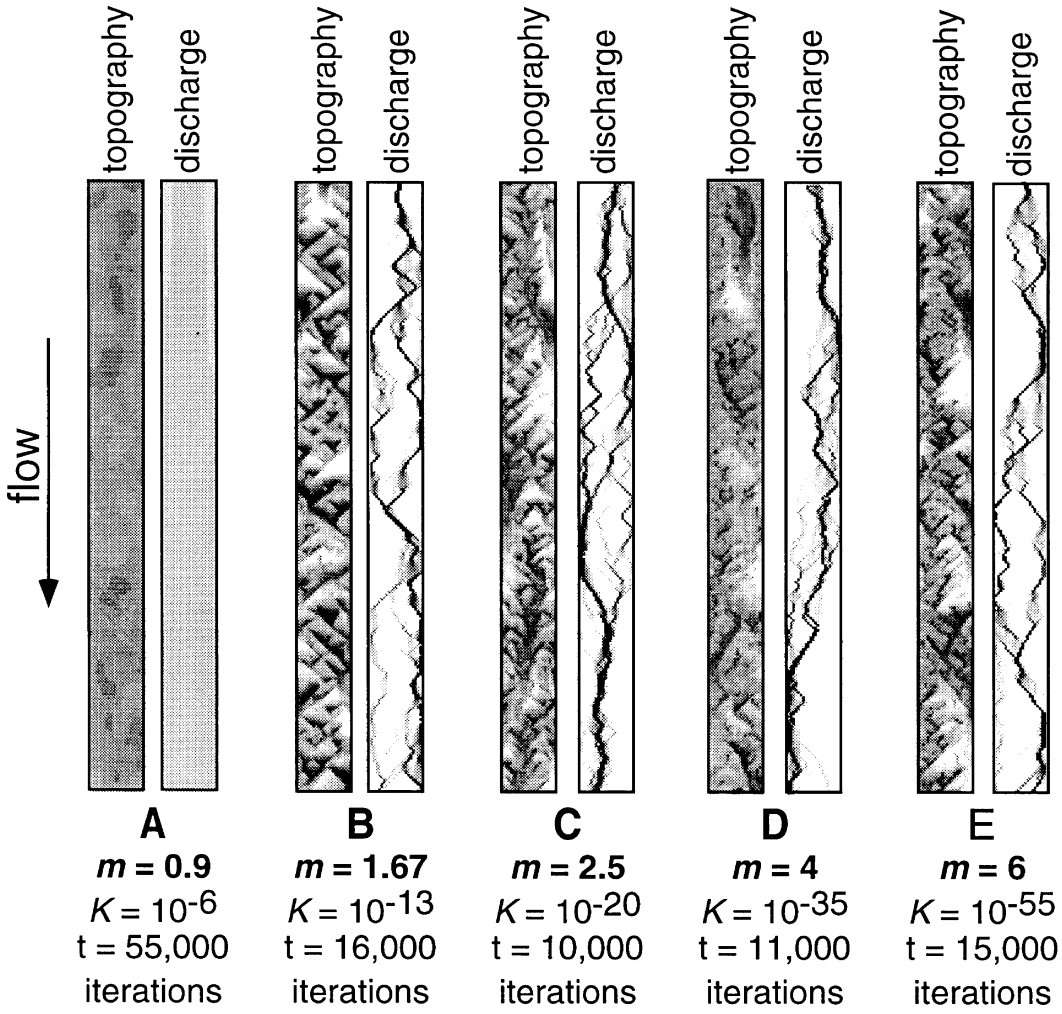

Figure 10. A series of model runs showing the effect of varying m, showing 22×250 cells. Darker shades indicate lower elevations and higher discharges. (In the topography image in (A), we use a grey scale that is more sensitive to small elevation changes than that used for all other runs, except where noted in Figure 12.) The overall slope has been removed before plotting the elevations. These runs used $n = 0{\cdot}5$, Q_s rule 3 with $C_s = 300\,000$, and $K_l = 10^{-7}$ in the lateral-sediment-transport (Q_l) rule.

depth) is approximately constant (the topographic perturbations change the details of the discharge distribution). We will show the results of using Q_s rule 3 in this experiment, but we have found qualitatively the same results using Q_s rule 4. The initially forming bars behave roughly as stability analyses predict, although, as can be expected, the bars are not as regular as those described by the analytical treatment. In a run with a confining channel four cells wide, the topographic highs and lows occur at the edges of the grid (Figure 12A). When the confining channel is eight cells wide, some of the bars are in the middle of the channel (Figure 12B). When the confining channel is twice as wide as this (16 cells) the number of early bars in a cross-section appears to be approximately doubled; the size and spacing of these bars appears to be the same as in the narrower cases (Figure 12C).

The development that occurs as the runs progress is also interesting. In a fully developed wider run, the number of channels in a cross-section carrying significant discharge (Figure 12D) is less than the number of thalwegs shown by the initially forming topography. Hence there is a tendency for channel coalescence to reduce the number of channels in a fully developed system relative to either the initial value or what would be predicted by stability theory.

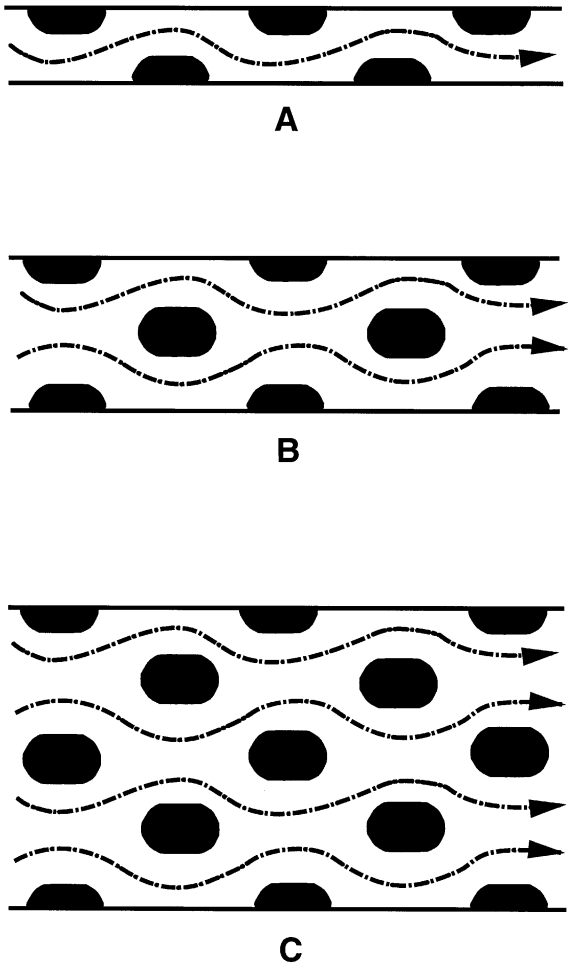

Figure 11. Schematic illustration of the effect of varying the width of a flow, keeping the average depth constant, predicted by linear stability analyses (Parker, 1976; Fredsoe, 1978). Dark areas represent the initially forming, infinitesimal-amplitude bars, and dotted lines represent the thalwegs between these bars.

In an experiment similar to this one, we started with a run in which discharge was introduced into the middle 12 cells in the first row (Figure 13A). In another run we doubled this number of cells in the first row receiving discharge, and also doubled the width of the confining channel, thus keeping the average discharge per cell constant. There are more channels per cross-section in the wider run (Figure 13B), but fewer than twice as many.

Effect of initial conditions

We have performed experiments using different initial conditions, such as: adding an erodible channel down the middle of the lattice that will convey the discharge initially, as is done in some laboratory models (Ashmore, 1985); adding a sinusoidal perturbation to the average cell heights; and various combinations of these two additions with different amplitudes and wavelengths for the sinusoidal component. As long as the lateral-sediment-transport rule is included, the flow regrades the topography until the elevation and discharge patterns are indistinguishable from those that result from the standard initial conditions. If the lateral-transport rule is not included in a run that starts with sinusoidal topography, narrow canyons cut through the high areas down to the level of the elevation troughs. The walls of these canyons never erode, and the pattern reaches a static steady state.

Figure 12. A series of model runs showing the effect of varying the width of the confining channel, introducing discharge in all the cells in the first row. Darker shades indicate lower elevations and higher discharges. (In the topography images in (A), (B) and (C) we use a grey scale that is more sensitive to small elevation changes than that used for all other runs, except where noted in Figure 10.) The overall slope has been removed before plotting the elevations. These runs used $n = 0{\cdot}5$, Q_s rule 3 with $m = 2{\cdot}5$, $C_s = 300\,000$, $K = 10^{-21}$, and $K_l = 10^{-7}$ in the lateral-sediment-transport (Q_l) rule.

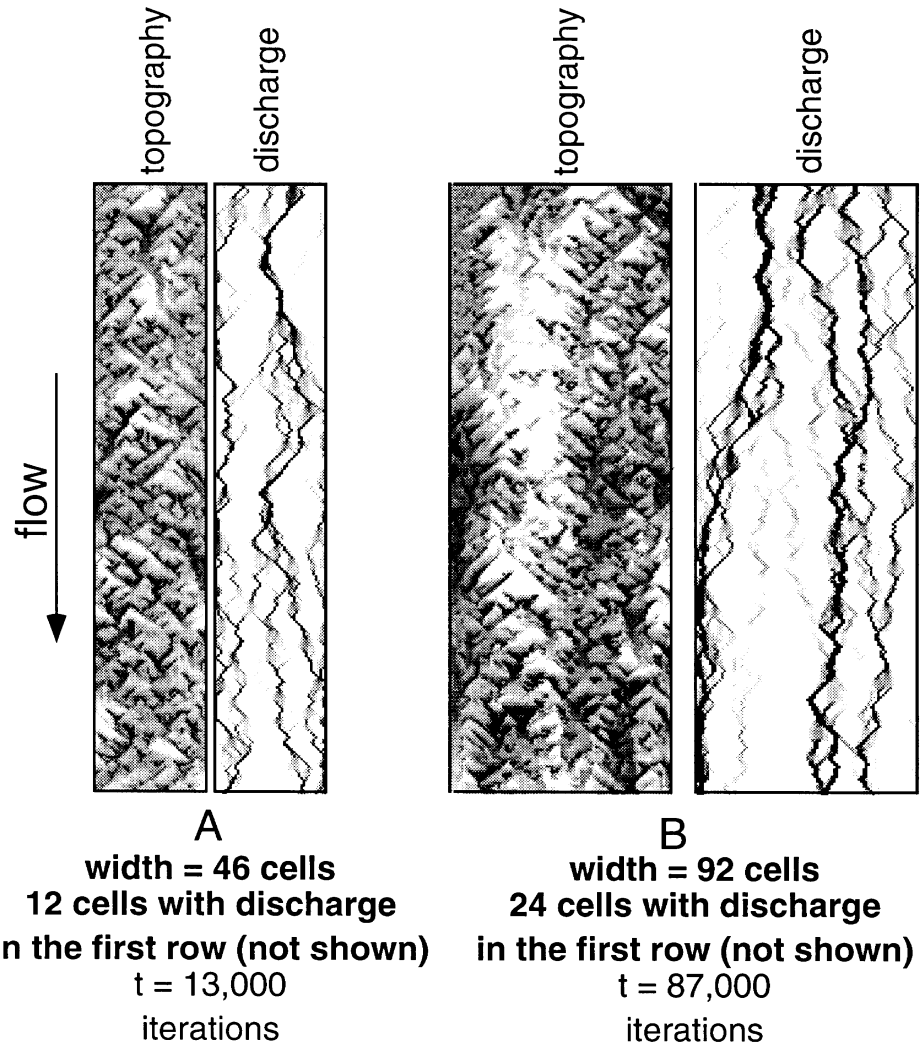

Figure 13. A pair of model runs in which we double the width of the confining channel and the number of cells in the first row receiving discharge. The lattice is 250 cells long. Darker shades indicate lower elevations and higher discharges. The overall slope has been removed before plotting the elevations. These runs used $n = 0{\cdot}5$, Q_s rule 3 with $m = 2{\cdot}5$, $C_s = 300\,000$, $K = 10^{-21}$, and $K_l = 10^{-7}$ in the lateral-sediment-transport (Q_l) rule.

Periodic sediment feed experiments

In a set of experiments to test how sediment pulses are transmitted downstream in the model, we fed into the upstream end of the lattice an amount of sediment that varied sinusoidally with time from 0 to the amount that would be transported on the average slope by a typical discharge. We used a single period for each run, with the periods ranging from 10 to 100 000 iterations. This longest period corresponds to roughly 100 days for a laboratory-scale physical braided-stream model, using the approximate scaling described above. We monitored the sediment flux past a cross-section 300 cells from the upstream end of the lattice, which corresponds to around 60 m in a laboratory-scale model.

Power spectra of the sediment-load time series for each run are all similar to that shown in Murray and Paola (1994); they show no obviously significant peaks. We wanted to see if a peak at the sediment feed frequency would develop for the longer-period runs. The system, however, does not transmit the signal downstream. In the

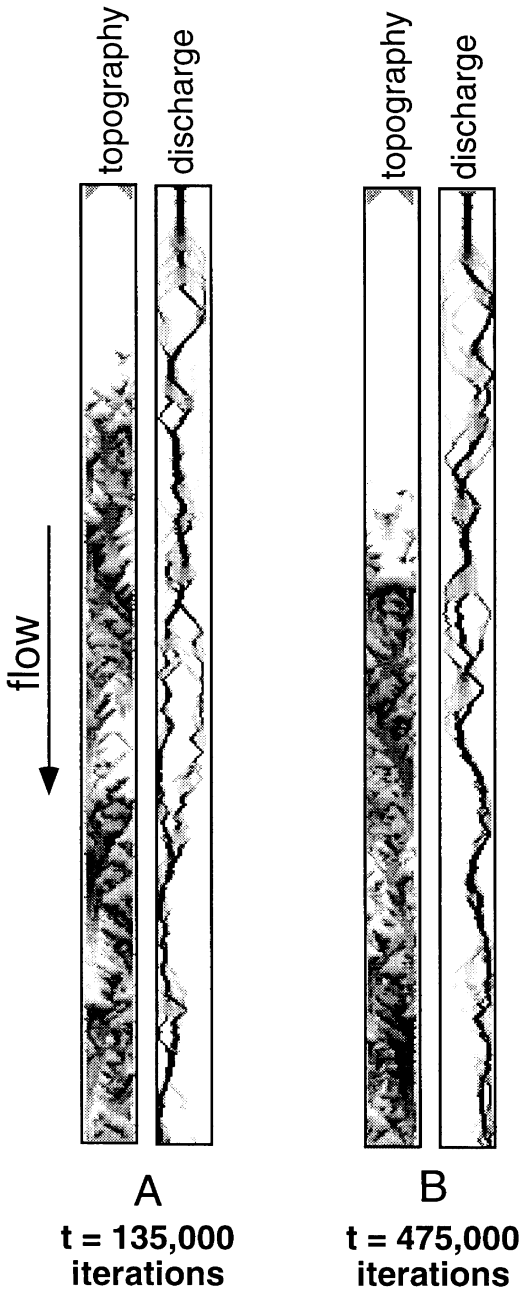

Figure 14. A run with a sinusoidally varying sediment feed, with a period of 10 000 iterations, showing 22×400 cells. Darker shades indicate lower elevations and higher discharges. The overall slope has been removed before plotting the elevations. This run used $n=0{\cdot}5$, Q_s rule 3 with $m=2{\cdot}5$, $C_s=300\,000$, $K=10^{-21}$, and $K_l=10^{-7}$ in the lateral-sediment-transport (Q_l) rule. (A) After 135 000 iterations, a large bar has built up near the top of the lattice. Dark areas near the downstream end of this bar show that the material in the bar is being reworked. (B) After 475 000 iterations that bar has become longer.

longer-period runs, a large bar approximately 100 cells long built up at the upstream end of the lattice during the high-feed part of each cycle (Figure 14), altering the slopes periodically in that region. If we had collected sediment at a cross-section in that region, we certainly would have detected the periodicity in the power spectrum. This bar, however, did not migrate downstream as a whole. During the low-feed part of each cycle,

channels cut into the deposit and moved some of the material downstream. The large bar grew longer as some of the reworked material was deposited nearby. However, this material did not continue to be transported as one obvious large mass. Instead, as it was eventually moved further downstream, it contributed to many bars that appeared to be similar to the bars that form during a standard run. In other words, the system destroys periodic input signals that are not long enough to cause the entire surface to regrade.

EROSION NETWORKS

The basic geometric difference between a static braid network and a typical dendritic erosional network is that the braid network includes confluences and bifurcations (diffluences) whilst the dendritic network has only confluences. We have carried out a series of experiments to see what would be needed to convert the braid pattern in our model into a dendritic pattern. These experiments have been done using basically the same methods as described above. The only differences are: (1) in the erosion experiments we make the lattice wider and shorter (Figure 15 shows 100×150 cells); and (2) we induce erosion by either adding a cliff at the downhill end or eliminating redeposition by disregarding sediment entering each cell. In constructing the cliff, we lower the last row of cells by 50 times the average elevation difference between rows. When we eliminate redeposition, we decrease the elevation of each cell according to the amount of material leaving during each iteration, changing Elev. rule 1 to:

$$\Delta Elev = -Q_s^{out} \qquad \text{(Elev. rule 2)}$$

so that cell elevation cannot increase.

When a cliff is added to the initial topography, knickpoints migrate upstream from the cliff, splitting along the way to create a dendritic channel pattern. Some of the channels that form in this way at the downhill end of the lattice disappear because their discharge is captured by the knickpoints of other channels. Some of the channels eventually extend themselves the length of the lattice. If lateral transport is not included, the pattern has then achieved a static steady state. If lateral transport is included a dendritic pattern forms, but the channel walls slowly erode, eventually leading to a dynamic braided pattern on a regraded slope.

When we eliminate sediment redeposition, an erosion pattern resembling rills develops (Figure 15C). In this case, the channels form anywhere on the lattice rather than at the downhill end. As the channels incise, no new splits in the flow form, although high areas in the initial topography can remain as islands. Again, the pattern reaches a static steady state. For reference, Figure 15D shows a real erosion pattern created in a laboratory-scale experiment (Schumm *et al*., 1987). In the experiment, water was sprayed over the whole surface, and not introduced only at the uphill end as in the model.

GEOMORPHIC IMPLICATIONS AND CONCLUSIONS

Minimal conditions for braiding

We quantitatively assess the model's realism elsewhere (Murray and Paola, 1996), finding that the model, while not completely realistic, produces spatial patterns similar to real rivers in ways that we believe reflect the processes involved. Regardless of the model's quantitative accuracy, we want to reiterate that we believe the most important result of this research is the model's qualitative success. Braided streams exhibit extremely complex spatial patterns and dynamics, perhaps suggesting that many complex processes or random influences must be invoked to explain braiding. The cellular model, however, seems to reproduce the essence of the dynamics using only simple, deterministic interactions between water and bedload sediment. This result suggests that much of the complexity of braiding may reflect the interplay of relatively simple processes. Braiding in the model requires, most importantly, a non-linear relationship between sediment flux and flow strength ($m>1$) that leads to excess scour at flow convergences and deposition at divergences. Robust, qualitatively realistic braiding in the model also requires sediment transport on flat or uphill surfaces and lateral sediment transport.

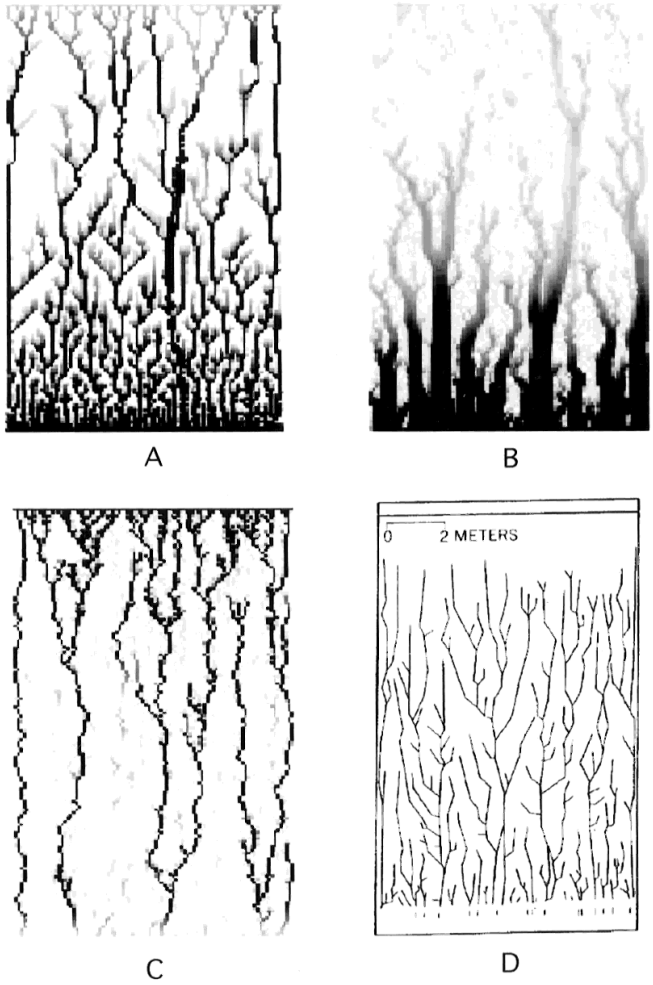

Figure 15. Erosion patterns, showing 100×150 cells. Darker shades indicate lower elevations. The overall slope has been removed before plotting the elevations. These runs used $n=0{\cdot}5$, Q_s rule 4 with $m=2{\cdot}5$, $\varepsilon=0{\cdot}35$, $K=10^{-21}$, and $K_l=10^{-7}$ in the lateral-sediment-transport (Q_l) rule (when included). In (A) and (B) a cliff with a height of 50 times the average difference between the elevations of adjacent rows was added to the downstream end of the initial topography. Lateral sediment transport is not included in (A) but is in (B). (C) Sediment redeposition is not included. No cliff was added to the topography, and lateral sediment transport was not included. (D) Experimental erosion pattern (Schumm *et al.*, 1987).

Different forms for the term that allows uphill transport (Q_s rules 3 and 4) produce patterns that differ in their details (Figures 5 and 6), raising questions about what aspects of the model output may be the artifacts of the particular rules used. However, we do not expect such a simple model to reproduce the exact behaviour of real rivers with either sediment-transport rule. Instead, our aim is to include in the model the most important processes in braiding, thereby producing the main dynamical characteristics of behaviour of real braided streams. In this sense, either form of the uphill-transport term seems sufficient.

Sediment-transport thresholds and stable-channel theory

Parker (1978) shows that a straight, uniform channel will adjust its width until the flow strength away from the banks is just above the threshold for sediment transport. Our model contains some of the interactions in a real stream that are important in this process, such as lateral transport. The model does not include the lateral diffusion of flow momentum into the channel banks, which Parker invoked to solve the stable channel paradox. Without this effect, a straight, uniform section of channel should widen itself until the flow conditions are below

the threshold everywhere (Parker, 1978). When a threshold is not included in the model, any straight, uniform channel sections should widen continually. If there were portions of the channel system that remained locally straight and uniform for a significant time, a run without a threshold should have some significantly wider channels than a run with a threshold. However, the addition of a threshold in Q_s rules 5 and 6 does not appear to change the channel widths in fully developed patterns, as the discharge patterns in Figures 5, 6 and 7 show. This result suggests that downstream convergence and divergence of flow, which are not included in the theories about straight, uniform channels, prevent the predicted adjustments between the sediment-transport threshold and channel width.

Erosion networks

The erosion experiments highlight the role of redeposition in braiding. Local deposition causes channel splitting; it leads to mid-channel bars (Ferguson, 1993) and to reoccupation of previous channels when the bed of a channel aggrades (Leddy *et al*., 1993). Braided networks result from the 'reversible' entrainment behaviour of cohesionless sediments, which are eroded and redeposited in response to local gradients in flow strength. Dendritic networks result when redeposition is removed from the rules, simulating the 'irreversible' entrainment of cohesive sediment as suspended or wash load, which, once eroded, cannot readily be redeposited (Partheniades, 1965). Erosion of narrow, deep channels upstream of a cliff makes redeposition ineffective, since enough local aggradation to fill the 'canyon' will not occur. Thus the changes that lead to erosional patterns involve suppressing redeposition either directly or indirectly (Figure 15). Without redeposition, once the flow gathers it can never split. The model results suggest that instead of the ongoing change of the braided system, static dendritic patterns develop without local redeposition.

Perhaps more importantly, these experiments show that the same model, with slight changes in the rules or the initial topography, can produce both behaviours. This 'erosional' version of our model does not contain the level of physical detail of recent simulations of landscape evolution (Willgoose *et al*., 1991; Rinaldo *et al*., 1993; Howard, 1994) but it does reveal the underlying unity between braided and dendritic systems. The fundamental factor that determines which will form seems to be sediment type. However, streams in non-cohesive sediment can develop dendritic networks if the system is strongly net erosional so that formation of bifurcations is suppressed.

Lateral sediment transport and bank erosion

In real braided rivers, as in the model, lateral sediment transport removes sediment from the banks, adding it to the sediment load in the channels, and widening the channels. The model results support the theory that lateral transport is important in braiding; in the model it plays a key role in producing qualitatively realistic braiding and dynamical behaviour, and maintaining that state indefinitely. Without this process, canyons – whether they erode back from a cliff as in the erosion-network experiments (Figure 15) or form spontaneously (Figure 8) – never decay. This result supports the natural supposition that cohesive channel banks are required to preserve an erosional canyon or dendritic pattern indefinitely.

Initial development versus final form

Linear stability analyses have been interpreted as distinguishing, based on width/depth ratio, whether a meandering or braided pattern will develop, and how many channels the stream will have (Parker, 1976; Fresdoe, 1978). Strictly, however, these analyses address only the initial developments that will occur in a flow that has some initial, well defined width/depth ratio, not the finite-amplitude, possibly emergent bars and separate channels of a fully developed braided stream. The model results we report here suggest that the number of channels in a fully developed stream may be smaller than the initial number of thalwegs (Figure 12). Although we have not performed a systematic investigation, our observations of laboratory experiments that start from a nearly smooth bed also suggest that the flow gathers into fewer, larger channels than form initially.

Extrapolating the predictions of stability analyses to the fully developed case, we would expect to see twice as many channels when we double the width of the confining channel and the number of cells receiving discharge. However, in the model, fewer than twice as many channels result (Figure 13). Field experiences lead us to suspect that this is consistent with real braided rivers; on a given slope, a river with a larger discharge

generally has larger, deeper channels, not just more channels the same size as in a river with a smaller discharge. A systematic study testing this idea would be interesting.

Time-varying sediment supply

Nicholas and others (in review) have used a one-dimensional model, without any flow convergence or divergence, to investigate how pulses of sediment are transmitted downstream. They found that, although diffused, the signals were transmitted downstream. In the varying-sediment-feed experiments with the cellular braided-stream model (Figure 14), however, we found that the signal was destroyed as the sediment moved downstream. The stepwise, intermittent transport and storage of material exhibited by the model is responsible for producing internally generated variations in sediment flux, as has been observed in real braided streams (Church and Jones, 1982; Ashmore, 1991). The results reported here suggest that braided rivers may act strongly as low-pass filters, at least for sediment-flux signals.

REFERENCES

Anderson, R. 1990. 'Eolian ripples as examples of self-organization in geomorphological systems', *Earth Science Reviews*, **28**(29), 77–96.

Ashmore, P. 1991. 'Channel morphology and bed load pulses in braided, gravel-bed streams', *Geografiska Annaler*, **73A**, 37–52.

Ashmore, P. E. 1985. *Process and form in gravel braided streams: laboratory modelling and field observations*, PhD thesis, University of Alberta.

Bagnold, R. A. 1980. 'An empirical correlation of bedload transport rates in natural rivers', *Proceedings of the Royal Society of London, Series A*, **372**, 453–473.

Barzini, G. N. and Ball, R. C. 1993. 'Landscape evolution in flood – a mathematical model', *Journal of Physics A: Math. Gen.*, **26**, 6777–6787.

Blondeaux, P. and Seminara, G. 1985. 'A unified bar-bend theory of river meanders', *Journal of Fluid Mechanics*, **157**, 449–470.

Chase, C. G. 1992. 'Fluvial landsculpting and the fractal dimension of topography', *Geomorphology*, **5**, 39–57.

Church, M. and Jones, D. 1982. 'Channel bars in gravel bed rivers', in Hey, R. D., Bathurst, J. C. and Thorne, C. R. (Eds) *Gravel-bed Rivers*, John Wiley & Sons, New York, 1982, 291–339.

Engelund, F. and Hansen, E. 1967. *A Monograph on Sediment Transport in Alluvial Streams*, Teknisk Forlag, Copenhagen, 62 pp.

Ferguson, R. I. 1993. 'Understanding braided processes in gravel-bed rivers: Progress and unsolved problems', in Best, J. L. and Bristow, C. S. (Eds), *Braided Rivers*, Geological Society, London, 73–87.

Forrest, S. B. and Haff, P. K. 1992. 'Mechanics of wind ripple stratigraphy', *Science*, **255**, 1240–1243.

Fredsoe, J. 1978. Meandering and braiding of rivers', *Journal of Fluid Mechanics*, **84**, 609–624.

Graf, W. H. 1971. *Hydraulics of Sediment Transport*, McGraw-Hill, New York.

Guckenheimer, J. and Holmes, P. 1983. *Nonlinear Oscillations, Dynamical Systems, and Bifurcations of Vector Fields*, Springer-Verlag, New York, 459 pp.

Hong, L. B. and Davies, T. R. H. 1979. 'A study of stream braiding', *Geological Society of America Bulletin, Part II*, **90**, 1839–1859.

Howard, A. D. 1994. 'A detachment-limited model of drainage basin evolution', *Water Resources Research*, **39**(7), 2261–2285.

Kaneko, K. 1993. *Theory and Applications of Coupled Map Lattices*, John Wiley and Sons, Chichester, 189 pp.

Leddy, J. O., Ashworth, P. J. and Best, J. L. 1993. 'Mechanisms of anabranch avulsion within gravel-bed braided rivers: observations from a scaled physical model', in Best J. L. and Bristow, C. S. (Eds), *Braided Rivers*, Geological Society, London, 119–127.

Lysne, D. K. 1969. 'Movement of sand in tunnels', *Journal of the Hydraulics Division, ASCE*, **95** (HY6), 1835–1846.

Murray, A. B. and Paola, C. 1994. 'A cellular model of braided rivers', *Nature*, **371**, 54–57.

Parker, G. 1976. 'On the cause and characteristic scales of meandering and braiding in rivers', *Journal of Fluid Mechanics*, **76**, 457–480.

Parker, G. 1978. 'Self-formed straight rivers with equilibrium banks and mobile bed. Part 2. The gravel river', *Journal of Fluid Mechanics*, **89**, 127–146.

Parker, G. 1984. Lateral bed load transport on side slopes', *Journal of Hydraulic Engineering*, **110**, 197–199.

Partheniades, E. 1965. 'Erosion and deposition of cohesive soils', *Journal of the Hydraulics Division, ASCE*, **91**(HY1), 105–139.

Rinaldo, A., Rodriguez-Iturbe, I., Rigon, R., Ijjasz-Vasquez, E. and Bras, R. L. 1993. 'Self-organized fractal river networks', *Physics Review Letters*, **70**(6), 822–825.

Schumm, S. A., Mosley, M. P. and Weaver, W. E. 1987. *Experimental Fluvial Geomorphology*, Wiley, New York, 413 pp.

Tetzlaff, D. M. and Harbaugh, J. W. 1989. *Simulating Clastic Sedimentation*, Van Nostrand Reinhold, New York, 196 pp.

Vernard, J. K. and Street, R. L. 1961. *Elementary Fluid Mechanics*, John Wiley & Sons, New York, 689 pp.

Werner, B. T. and Fink, T. M. 1993. Beach cusps as self-organized patterns', *Science*, **260**, 968–971.

Werner, B. T. and Hallet, B. 1993. Numerical simulation of self-organized stripes', *Nature*, **361**, 142–145.

Willgoose, G., Bras, R. L. and Rodriguez-Iturbe, I. 1991. A coupled channel network growth and hillslope evolution model. I. Theory', *Water Resources Research*, **27**(7), 1671–1684.

Wolfram, S. 1984. 'Universality and complexity in cellular automata', *Physica*, **10D**, 1–35.

